Nonlinear-response properties in a simplified time-dependent density functional theory (sTD-DFT) framework: Evaluation of the first hyperpolarizability

Marc de Wergifosse, and Stefan Grimme

Citation: The Journal of Chemical Physics **149**, 024108 (2018); doi: 10.1063/1.5037665
View online: https://doi.org/10.1063/1.5037665
View Table of Contents: http://aip.scitation.org/toc/jcp/149/2
Published by the American Institute of Physics

Nonlinear-response properties in a simplified time-dependent density functional theory (sTD-DFT) framework: Evaluation of the first hyperpolarizability

Marc de Wergifosse[a] and Stefan Grimme
Mulliken Center for Theoretical Chemistry, Institut für Physikalische und Theoretische Chemie, Beringstr. 4, 53115 Bonn, Germany

(Received 26 April 2018; accepted 20 June 2018; published online 13 July 2018)

Recent developments in nonlinear imaging microscopy show the need to implement new theoretical tools, which are able to characterize nonlinear optical properties in an efficient way. For second-harmonic imaging microscopy (SHIM), quantum chemistry could play an important role to design new exogenous dyes with enhanced first hyperpolarizabilities or to characterize the response origin in large endogenous biological systems. Such methods should be able to screen a large number of compounds while reproducing their trends and to treat large systems in reasonable computation times. To fulfill these requirements, we present a new simplified time-dependent density functional theory (sTD-DFT) implementation to evaluate the first hyperpolarizability where the Coulomb and exchange integrals are approximated by short-range damped Coulomb interactions of transition density monopoles. For an ultra-fast computation of the first hyperpolarizability, a tight-binding version (sTD-DFT-xTB) is also proposed. In our implementation, a sTD-DFT calculation is more than 600 time faster with respect to a regular TD-DFT treatment, while the xTB version speeds up the entire calculation further by at least two orders of magnitude. We challenge our implementation on three test cases: typical push-pull π-conjugated compounds, fluorescent proteins, and a collagen model, which were selected to model requirements for SHIM applications. *Published by AIP Publishing.* https://doi.org/10.1063/1.5037665

I. INTRODUCTION

Characterizing theoretically nonlinear optical properties of compounds useful for nonlinear imaging microscopy such as multicolor two-photon imaging microscopy (M2PIM)[1] or second harmonic imaging microscopy (SHIM)[2] is a real challenge for quantum chemistry where new methods need to be implemented and tested. These two imaging techniques are based on nonlinear optical phenomena: two-photon absorption (2PA) (and emission) and second-harmonic generation (SHG).[3,4] SHIM of biological tissues requires endogenous and/or exogenous dyes with large first hyperpolarizability (β). Endogenous dyes encompass many different types of structural proteins where their molecular arrangements can be probed by SHIM. Among endogenous dyes, collagen is probably the most important one for the diagnosis of tissue alteration due to diseases.[5] For example, in case of fibrosis, the three-dimensional distribution of collagen is modified and fibrillar collagen accumulates in the tissue. In the case of exogenous dyes, molecular properties need to be carefully adjusted to provide dyes with, e.g., limited phototoxicity.[6] The desired main properties are (i) a large first hyperpolarizability at the wavelength of illumination to maximize the signal, (ii) charge transfer bands enhanced at approximately the wavelength (one-photon enhancement) and half the wavelength (two-photon enhancement) in the biological tissue transparency window (700-900 nm), to achieve resonance enhancement, (iii) a high affinity for biological membranes, and (iv) the ability to aggregate in a non-centrosymmetric way since centrosymmetric structures have no SHG responses. Amphiphilic dyes are well suited to satisfy conditions (iii) and (iv). Biological systems contain membranes and interfacial structures, which are asymmetric environments and are therefore favorable to organize the chromophores, leading to constructive interferences and enhanced SHG responses. Unfortunately, condition (ii) is counterproductive with respect to the design of dyes exhibiting limited photodamage. Most of SHG exogenous probes currently used for SHIM can lead to photodamage[7,8] where their SHG signals are always accompanied by two-photon fluorescence[9,10] indicating that the excited states are populated via a multi-photon process. This demonstrates the need for designing new dyes with large SHG responses since they could be detected with smaller laser intensities as well as low or non-existent 2PA activity in the experimental range of frequencies.

Designing new SHIM dyes or rationalizing the response origin in endogenous biological structures could benefit from a fast and systematic quantum chemical evaluation of β. But predicting the β value of molecules and matter is, however, a challenging task, owing to many subtle issues that need to be considered. The description of the first hyperpolarizability requires accurate quantum chemistry methods accounting for (i) electron correlation effects, (ii) proper frequency dispersion, and (iii) environment effects.[11,12] Concerning

[a]Author to whom correspondence should be addressed: mdewergifosse@gmail.com

electron-correlation effects, two major types of methods are usually employed to evaluate β: wave function methods and density functional theory (DFT) approaches. Due to their computational requirements, wave function methods can only be applied to relatively small systems. They can be used as reference methods in order to assess the reliability of DFT used with different approximate exchange-correlation (XC) functionals.[13–16] Among wave function methods, de Wergifosse and Champagne[13] showed that the MP2 method predicts β of push-pull π-conjugated systems with an accuracy similar to coupled cluster singles and doubles calculations with a perturbative estimate of triples [CCSD(T)]. MP2 can treat medium-sized systems, but usually only the static value for β is obtained using finite-field perturbation theory.[17] In that case, approximate schemes have been developed where the static β value is calculated at a correlated level, while the frequency dispersion is estimated at a lower theory level, typically using the time-dependent Hartree-Fock (TDHF) scheme. Carefully used, TD-DFT (time-dependent density functional theory) can provide an efficient way to determine nonlinear properties for medium to large systems but sometimes for non-negligible computational costs. This implies a wise selection of the XC functional and the basis set. In the case of push-pull π-conjugated compounds, de Wergifosse and Champagne[13] showed that among XC correlation functionals, the long-range corrected LC-BLYP functional (LC-BLYP) seems the most reliable to characterize trends for a set of molecules in a systematic manner. Solvent effects are commonly accounted for by using continuum models. However, the reliability of implicit solvation models was recently challenged by comparison against an explicit scheme where the solvent molecules are represented by point charges,[18–20] and where the first solvation shell is considered explicitly in the QM calculation as well.[19] It was shown that β calculated with the implicit solvation model are usually larger than those obtained with the multiscale approach.[18] The effects of the environment can also be treated explicitly using the ONIOM (our own N-layered integrated molecular orbital and molecular mechanics) method,[21] where the system is divided into successive layers: the core layer, which should be treated at the highest level of approximation (quantum level with electron correlation) and the outermost layer that can be treated at a low level (semi-empirical Hamiltonian or Hartree-Fock level). In studies on fluorescent proteins,[22,23] de Wergifosse *et al.* showed that in order to achieve quantitative agreement with experiment, electron correlation is crucial to get accurate molecular first hyperpolarizabilities as well as to describe the first shell of residues (amino acids and water molecules) involving H-bonds and van der Waals interactions.

The aim of this article is to introduce a new simplified TD-DFT formulation to evaluate first hyperpolarizabilities, providing a fast and efficient method able to screen large numbers of compounds and to treat very large molecular systems. The density-matrix based linear and nonlinear-response TD-DFT formalism[24–30] is modified in the same sTD-DFT (simplified TD-DFT) framework as proposed by Grimme and co-workers[31–33] for the determination of electronic excitation spectra of very large molecules. This formalism is also extended to an existing tight-binding based sTD-DFT approximation (sTD-DFT-xTB), following the method proposed by Grimme and Bannwarth.[33] A similar scheme was proposed by Nénon and Champagne[34,35] using the SCC-DFTB (self-consistent charge density functional tight-binding) method. Though, only the evaluation of the static property was done using a finite-field method. After a recapitulation of the density-matrix based linear and nonlinear-response TD-DFT formalism and its sTD-DFT counterpart in Sec. II, three challenging cases are tested: push-pull π-conjugated compounds,[13,36] fluorescent proteins,[22,23,37] and a collagen model,[38] comprising more than 1035 atoms in the largest system considered. Section III gives details about the implementation, systems, and computations, Sec. IV contains the results, and conclusions and outlooks are outlined in Sec. V.

II. THEORY

A. Linear and quadratic-response TD-DFT

The sTD-DFT method to evaluate the first hyperpolarizability employs the density-matrix based linear and nonlinear-response TD-DFT formalism.[24–30] The popular Tamm-Dancoff approximation introduced by Hirata and Head-Gordon[25] in the quantum chemistry community was formulated in this framework, which was extended to linear and nonlinear responses by Furche.[26] We are following the derivation of Zahariev and Gordon[29] that was implemented in GAMESS,[39,40] in 2014. Recently, Furche and co-workers[30] reported a TURBOMOLE[41] implementation using a similar formalism. In the following, p, q, r, s indices refer to general molecular orbitals, i, j, k, l to occupied, and a, b, c, d to unoccupied molecular orbitals.

Prior to applying any perturbation, the system belongs to its ground state where the one-electron density matrix $\rho(\mathbf{r}, \mathbf{r}')$ is developed in the Kohn-Sham spin-orbitals $\phi_p(\mathbf{r})$,

$$\rho(\mathbf{r}, \mathbf{r}') = \sum_{pq} D_{pq}\phi_p(\mathbf{r})\phi_q^*(\mathbf{r}'), \tag{1}$$

where D_{pq} is a one-particle density matrix component in this representation. When applying a perturbation, the time evolution of the discrete-index representation of the density matrix obeys to the Heisenberg equation-of-motion

$$i\frac{\partial D_{pr}}{\partial t} = \sum_q (F_{pq}^{KS} D_{qr} - D_{pq}F_{qr}^{KS}), \tag{2}$$

where $\mathbf{F}^{KS}$ is the Kohn-Sham equivalent to the Fock matrix. Suppose that the system is perturbed by an external monochromatic oscillating electric field at a frequency ω,

$$\vec{F}(t) = \vec{f}(\omega)[e^{-i\omega t} + e^{i\omega t}], \tag{3}$$

with field amplitudes $\vec{f}(\omega)$. The time-dependent perturbation reads

$$V_{pq}(t) = \lambda[h_{pq}e^{-i\omega t} + h_{pq}^* e^{i\omega t}], \tag{4}$$

where $h_{pq} = \sum_\zeta^{x,y,z} f_\zeta(\omega)\langle\phi_p|\hat{\mu}_\zeta|\phi_q\rangle$ and λ is a dimensionless coupling strength. Note that considering a monochromatic electric field leads naturally to the linear case. The time evolution of the density matrix and the Fock matrix are expressed as perturbation expansion

$$D_{pq} = D_{pq}^{(0)} + \lambda D_{pq}^{(1)} + \lambda^2 D_{pq}^{(2)} + \cdots, \tag{5}$$

$$F_{pq}^{KS} = F_{pq}^{(0)} + \lambda F_{pq}^{(1)} + \lambda^2 F_{pq}^{(2)} + \cdots. \tag{6}$$

Setting $\lambda = 1$, inserting (5) and (6) into the equation-of-motion (2), and solving it for the first-order perturbation using idempotence relations lead to the linear response TD-DFT equation

$$i\frac{\partial D_{pr}^{(1)}}{\partial t} = \sum_q (F_{pq}^{(1)} D_{qr}^{(0)} - D_{pq}^{(0)} F_{qr}^{(1)}) + \sum_q (F_{pq}^{(0)} D_{qr}^{(1)} - D_{pq}^{(1)} F_{qr}^{(0)}), \tag{7}$$

where the linear response of the density matrix is expressed as

$$D_{pq}^{(1)} = [d_{pq} e^{-i\omega t} + d_{pq}^* e^{i\omega t}]. \tag{8}$$

Note that only occupied-unoccupied and unoccupied-occupied density matrix blocks are nonzero. The first-order response of the Fock matrix reads

$$F_{pq}^{(1)} = V_{pq}(t) + \sum_{r,s} \frac{\partial F_{pq}}{\partial D_{rs}} D_{rs}^{(1)}. \tag{9}$$

Equations (8) and (9) are combined into (7) and by collecting terms in $e^{-i\omega t}$ and in $e^{i\omega t}$, the linear-response matrix equation is obtained,

$$\left[\begin{pmatrix} \mathbf{A} & \mathbf{B} \\ \mathbf{B}^* & \mathbf{A}^* \end{pmatrix} - \omega \begin{pmatrix} 1 & 0 \\ 0 & -1 \end{pmatrix}\right]\begin{pmatrix} \mathbf{X}(\omega) \\ \mathbf{Y}(\omega) \end{pmatrix} = \begin{pmatrix} \mathbf{h} \\ \mathbf{h} \end{pmatrix}, \tag{10}$$

where one defines $X_{ai} = d_{ai}$ and $Y_{ai} = d_{ia}$,

$$A_{ia,jb} = \delta_{ij}\delta_{ab}(\epsilon_a - \epsilon_i) + 2(ia|jb) - a_x(ij|ab) + (1 - a_x)(ia|f_{XC}|jb), \tag{11}$$

and

$$B_{ia,jb} = 2(ia|bj) - a_x(ib|aj) + (1 - a_x)(ia|f_{XC}|bj). \tag{12}$$

A and **B** components have been written for a global hybrid density functional in the singlet restricted case. Here, a_x is the amount of Fock exchange, ϵ_p is the energy of the p orbital, $(ia|jb)$, $(ia|bj)$, and $(ib|aj)$ are exchange type integrals in the Mulliken notation, $(ij|ab)$ is a Coulomb-type integral, and $(ia|f_{XC}|jb)$ and $(ia|f_{XC}|bj)$ are the responses of the exchange-correlation functional. Note that by switching off the perturbation, Eq. (10) leads to the usual TD-DFT matrix equation to compute excited state energies and eigenvectors. Equation (10) is reformulated by assuming that the orbitals used are real and by taking its first derivative with respect to the external applied electric field ($\frac{\partial}{\partial F_\zeta}|_{\vec{F}=0}$),

$$\left[\begin{pmatrix} \mathbf{A} & \mathbf{B} \\ \mathbf{B} & \mathbf{A} \end{pmatrix} - \omega \begin{pmatrix} 1 & 0 \\ 0 & -1 \end{pmatrix}\right]\begin{pmatrix} \mathbf{X}_\zeta(\omega) \\ \mathbf{Y}_\zeta(\omega) \end{pmatrix} = -\begin{pmatrix} \mu_\zeta \\ \mu_\zeta \end{pmatrix}, \tag{13}$$

where the derivative of the first-order perturbation of the density matrix defines the frequency-dependent response vectors $\frac{\partial D_{ai}^{(1)}(\omega)}{\partial F_\zeta}|_{\vec{F}=0} = X_{\zeta,ai}(\omega) + Y_{\zeta,ai}(\omega)$ and where $\mu_{\zeta,ai} = \langle \phi_a | \hat{\mu}_\zeta | \phi_i \rangle$. When considering a monochromatic perturbation, the time evolution of the electric dipole moment depends on the polarizability tensor, $\overleftrightarrow{\alpha}(-\omega;\omega)$. Since the perturbation expansion of the electronic component of the dipole moment is expressed as

$$\mu_\zeta(t) = -2\left[\sum_{pq} \mu_{\zeta,pq} D_{pq}^{(0)} + \sum_\omega \sum_\eta^{x,y,z} \sum_{pq} \mu_{\zeta,pq} \frac{\partial D_{pq}^{(1)}(\omega)}{\partial F_\eta}|_{\vec{F}=0} f_\eta(\omega) e^{\pm i\omega t} + \frac{1}{2!} \sum_{\omega_1,\omega_2} \sum_{\eta,\xi}^{x,y,z} \sum_{pq} \mu_{\zeta,pq} \frac{\partial^2 D_{pq}^{(2)}(\omega_1,\omega_2)}{\partial F_\eta \partial F_\xi}|_{\vec{F}=0} f_\eta(\omega_1) f_\xi(\omega_2) e^{\pm i\omega_\sigma t} + \cdots\right], \tag{14}$$

and that the Taylor expansion of the time-dependent dipole moment reads

$$\mu_\zeta(t) = \mu_\zeta(0) + \sum_\omega \sum_\eta^{x,y,z} \alpha_{\zeta\eta}(-\omega;\omega) f_\eta(\omega) e^{\pm i\omega t} + \frac{1}{2!} \sum_{\omega_1,\omega_2} \sum_{\eta,\xi}^{x,y,z} \beta_{\zeta\eta\xi}(-\omega_\sigma;\omega_1,\omega_2) \times f_\eta(\omega_1) f_\xi(\omega_2) e^{\pm i\omega_\sigma t} + \cdots, \tag{15}$$

a component of the polarizability tensor is defined as

$$\alpha_{\zeta\eta}(-\omega;\omega) = -2\sum_{ai} \mu_{\zeta,ai} \frac{\partial D_{ai}^{(1)}(\omega)}{\partial F_\eta}|_{\vec{F}=0} = -2\sum_{ai} \mu_{\zeta,ai}(X_{\eta,ai}(\omega) + Y_{\eta,ai}(\omega)). \tag{16}$$

The linear response vectors at a frequency ω necessary to evaluate the polarizability are obtained as

$$\mathbf{X}_\zeta(\omega) + \mathbf{Y}_\zeta(\omega) = \frac{-2\mu_\zeta}{(\mathbf{A}+\mathbf{B}) - \omega^2(\mathbf{A}-\mathbf{B})^{-1}}. \tag{17}$$

In the case of two incident photons, ω_1 and ω_2, the dipole moment quadratic response is described by the first hyperpolarizability tensor, $\overleftrightarrow{\beta}(-\omega_\sigma;\omega_1,\omega_2)$. To obtain this quantity, one needs to evaluate the quadratic-response TD-DFT equation obtained by solving the Heinsenberg equation-of-motion for the second-order to obtain quadratic response vectors. This can be alleviate by using the "(2n + 1)" theorem and only evaluating linear-response vectors calculated for three different frequencies: ω_1, ω_2, and $-\omega_\sigma = -\omega_1 - \omega_2$. The derivation of the first hyperpolarizability component, $\beta_{\xi\zeta\eta}(-\omega_\sigma;\omega_1,\omega_2)$, in terms of linear-response vectors is out of the scope

of this paper, but the interested reader can follow the progression of Zahariev and Gordon,[29] further information can be gathered from the seminal paper by Furche[26] and a paper by Wang *et al.*[27] The linear-response solution of the first hyperpolarizability reads

$$\beta_{\xi\zeta\eta}(-\omega_\sigma;\omega_1,\omega_2) = A - B + C, \tag{18}$$

$$A = \sum_{perm.\xi,\zeta,\eta}\left\{\sum_{aij} X_{\xi,ai}(-\omega_\sigma)\left[-\mu_{\zeta,ij} + \sum_{ck} f^{HXC}_{ij,ck}\left(X_{\zeta,ck}(\omega_1) + Y_{\zeta,ck}(\omega_1)\right)\right]Y_{\eta,aj}(\omega_2)\right\}, \tag{19}$$

$$B = \sum_{perm.\xi,\zeta,\eta}\left\{\sum_{iab} X_{\xi,ai}(-\omega_\sigma)\left[-\mu_{\zeta,ab} + \sum_{ck} f^{HXC}_{ab,ck}\left(X_{\zeta,ck}(\omega_1) + Y_{\zeta,ck}(\omega_1)\right)\right]Y_{\eta,bi}(\omega_2)\right\}, \tag{20}$$

$$C = \sum_{perm.\xi,\zeta,\eta}\left\{\sum_{aibjck} g^{XC}_{ai,bj,ck}(X_{\xi,ai}(-\omega_\sigma) + Y_{\xi,ai}(-\omega_\sigma)) \times (X_{\zeta,bj}(\omega_1) + Y_{\zeta,bj}(\omega_1))(X_{\eta,ck}(\omega_2) + Y_{\eta,ck}(\omega_2))\right\}, \tag{21}$$

where "$perm.\xi,\zeta,\eta$" is related to the inclusion of six permutations of indices (and related frequencies) into the summation. $f^{HXC}_{ij,ck}$ is the Hartree exchange-correlation kernel,

$$f^{HXC}_{ij,ck} = 2(ij|ck) - a_x(jk|ci) + (1-a_x)(ij|f_{XC}|ck), \tag{22}$$

and $g^{XC}_{ai,bj,ck}$ is the third functional derivative of the exchange-correlation functional.

B. Simplified TD-DFT approaches

Following the simplified approach used in sTDA[31,33] and sTD-DFT,[32] three modifications are applied in the linear response TD-DFT equation (13). First, the response of the exchange-correlation functional is neglected in **A** and **B** matrices. Second, the Coulomb and exchange integrals are approximated by short-range damped Coulomb interactions of transition density monopoles. While a Löwdin population analysis determines transition charge densities q^A_{pq} centered on atom A, the two-electron integrals are approximated by

$$(pq|rs)' = \sum_A^N \sum_B^N q^A_{pq} q^B_{rs} \Gamma_{AB}, \tag{23}$$

where Γ_{AB} is the Mataga-Nishimoto-Ohno-Klopman (MNOK)[42–44] damped Coulomb operator. For Coulomb integrals $(ij|ab)'_J$, the MNOK operator takes the form

$$\Gamma^J_{AB} = \left(\frac{1}{(R_{AB})^{y_J} + (a_x\eta)^{-y_J}}\right)^{\frac{1}{y_J}}, \tag{24}$$

where R_{AB} is the interatomic distance, y_J is a parameter, and η is the chemical hardness mean of atoms A and B. The MNOK operator is slightly different for approximated exchange integrals $(ia|jb)'_K$,

$$\Gamma^K_{AB} = \left(\frac{1}{(R_{AB})^{y_K} + \eta^{-y_K}}\right)^{\frac{1}{y_K}}, \tag{25}$$

where y_K is another parameter. Simple linear relations determine y_J and y_K parameters in the a_x range from 0 to 1.[31] The chemical hardness values used are tabulated for all elements.[45] The **A** and **B** matrix elements are then approximated by

$$A'_{ia,jb} = \delta_{ij}\delta_{ab}(\epsilon_a - \epsilon_i) + 2(ia|jb)'_K - (ij|ab)'_J, \tag{26}$$

$$B'_{ia,jb} = 2(ia|bj)'_K - a_x(ib|aj)'_K. \tag{27}$$

Note that the amount of Hartree-Fock exchange is not appearing anymore in Eq. (26) though, the MNOK Coulomb operator implicitly incorporates it. The third simplification concerns the truncation of the CI space which is controlled by a single energy cut-off parameter; for details, see the original sTDA publication.[31] The implication of this will be discussed in Sec. IV.

The linear-response vectors used in the sTD-DFT method to compute the polarizability and the first hyperpolarizability are obtained by the sTD-DFT equivalent of Eq. (17),

$$\mathbf{X}'_\zeta(\omega) + \mathbf{Y}'_\zeta(\omega) = \frac{-2\boldsymbol{\mu}_\zeta}{(\mathbf{A}'+\mathbf{B}') - \omega^2(\mathbf{A}'-\mathbf{B}')^{-1}}. \tag{28}$$

The polarizability is then determined by

$$\alpha'_{\zeta\eta}(-\omega;\omega) = -2\sum_{ai}\mu_{\zeta,ai}(X'_{\eta,ai}(\omega) + Y'_{\eta,ai}(\omega)). \tag{29}$$

For the first hyperpolarizability, we only consider the second-harmonic generation case $[\vec{\beta}'(-2\omega;\omega,\omega)]$ where the two incident frequencies are degenerate. To reduce the computational cost of the method, the sTD-DFT evaluation of the first hyperpolarizability needs two extra simplifications: first, the C term in Eq. (18) is dropped and second, the f^{HXC} terms in both A and B equations are neglected. For the second approximation, if one wants to keep the f^{HXC} kernel, two new groups of three-center two-electron integrals need to be parameterized. Since we are aiming for a simple and fast method with as few parameters as possible, these two approximations represent a reasonable compromise. Note that a reparameterization of y_J and y_K could encompass some effects of these simplifications. The impact of this is discussed for two push-pull π-conjugated compounds in Sec. IV A. The linear-response solution of the second-harmonic generation first hyperpolarizability in the sTD-DFT approximations reads

$$\beta'_{\xi\zeta\eta}(-2\omega;\omega,\omega) = A' - B', \tag{30}$$

$$A' = \sum_{perm.\xi,\zeta,\eta}\left\{\sum_{aij} X'_{\xi,ai}(-2\omega)\left[-\mu_{\zeta,ij}\right]Y'_{\eta,aj}(\omega)\right\}, \tag{31}$$

$$B' = \sum_{perm.\xi,\zeta,\eta}\left\{\sum_{iab} X'_{\xi,ai}(-2\omega)\left[-\mu_{\zeta,ab}\right]Y'_{\eta,bi}(\omega)\right\}. \tag{32}$$

In addition, we interface the above described sTD-DFT scheme with the xTB tight-binding method,[33] providing an unprecedented ultra-fast approach to the second-harmonic

generation response for large systems (sTD-DFT-xTB approximation). See Ref. 33 for more information about sTD-DFT-xTB for the calculation of excitation spectra. Briefly, in this method, the KS-DFT orbitals and eigenvalues are replaced by corresponding data from an extended basis set tight-binding calculation.

III. COMPUTATIONAL DETAILS

The sTD-DFT linear and quadratic responses are implemented in the sTDA program.[31] To obtain the linear-response vectors $\mathbf{X}'_\zeta(\omega)$ and $\mathbf{Y}'_\zeta(\omega)$ for a frequency ω, one only needs to invert two matrices. For a list of frequencies, the program inverses $(\mathbf{A}'-\mathbf{B}')$ once and $[(\mathbf{A}'+\mathbf{B}')-\omega^2(\mathbf{A}'-\mathbf{B}')^{-1}]$ for each frequency. When calculating the SHG first hyperpolarizability, the linear-response vectors are computed for ω and -2ω. For the static case, Kleinman's conditions[46] are applied to reduce the computational cost, where only ten tensor components are calculated. In the frequency domain, the SHG β tensor still has some symmetries because of the two degenerated frequencies. There, we calculate 18 different tensor components.

We tested our implementation on three challenging cases. The first one considers a set of six push-pull π-conjugated molecules (Fig. 1). Four of these molecules were investigated by de Wergifosse and Champagne in 2011 to assess electron correlation effects on the first hyperpolarizability:[13] $(H_3C)_2N-(CH=CH)_6-NO_2$ [m−3], $(H_3C)_2N-(C\equiv C)_6-NO_2$ [m−4], *N*,*N*-dimethyl-4-(4-nitrophenyl)aniline [m−5], and *N*,*N*-dimethyl-5-(5-nitrothiophen-2-yl)thiophen-2-amine [m−6]. Two smaller molecules were investigated at the CCSD level of theory assessing frequency-dispersion effects:[36] $H_2N-CH=CH-CH=CH-NO_2$ [m−1] and

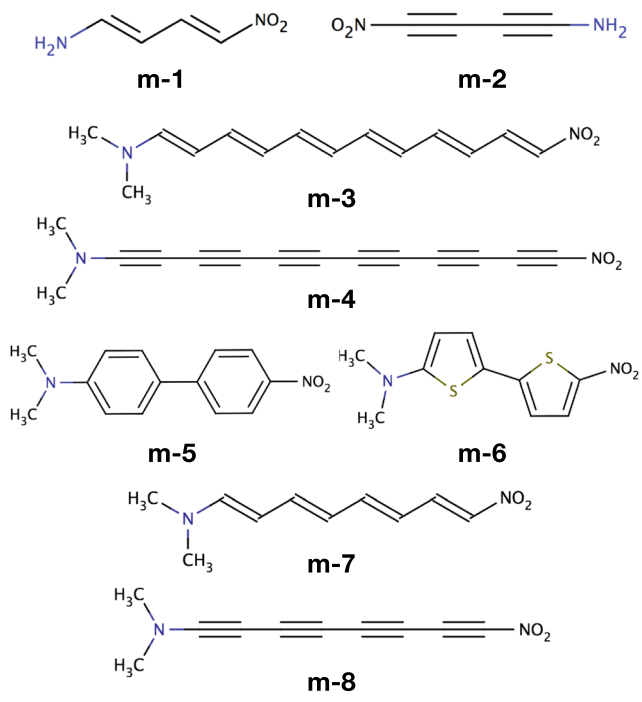

FIG. 1. First case study: the eight push-pull π-conjugated molecules.

$H_2N-C\equiv C-C\equiv C-NO_2$ [m−2]. We used the same geometries as in these previous studies.[13,36] The reference TD-DFT calculations were done using the BHandHLYP[47] functional with the 6-31G(d)[48] and 6-31+G(d)[49] Gaussian basis sets and compared to sTD-DFT results. Reference values were taken from Refs. 13 and 36 and compared to sTD-DFT-xTB results. This includes MP2, CCSD, and CCSD(T) data. In the comparison with xTB, we have included two extra

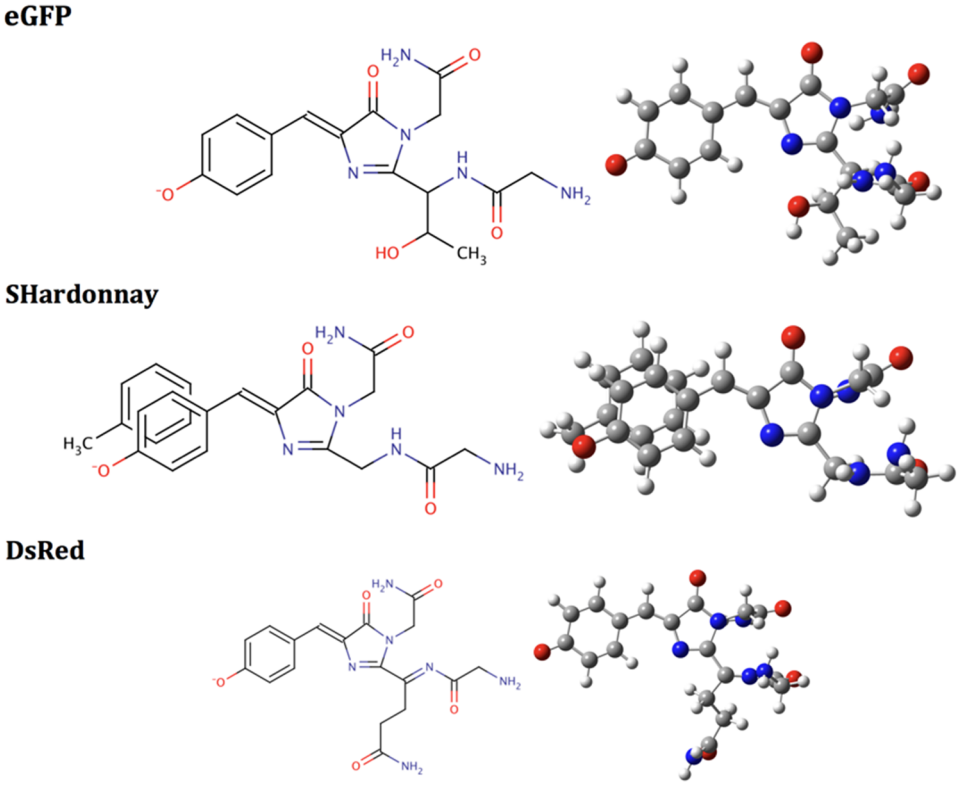

FIG. 2. Molecules in the second case study: the three fluorescent protein chromophores.

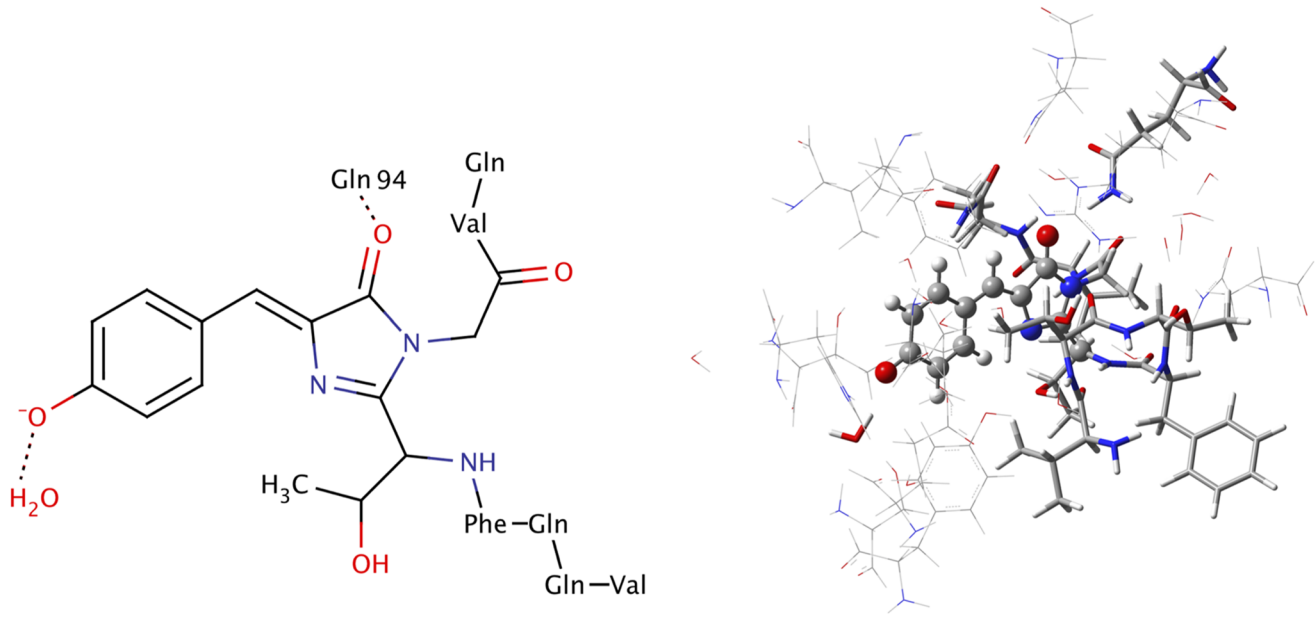

FIG. 3. Molecules used in the second case study: eGFP chromophore and part of its first shell of residues. The sketched picture corresponds to the high ONIOM layer and the "ball-and-stick" image to the full system considered where the low layer appeared in wires.

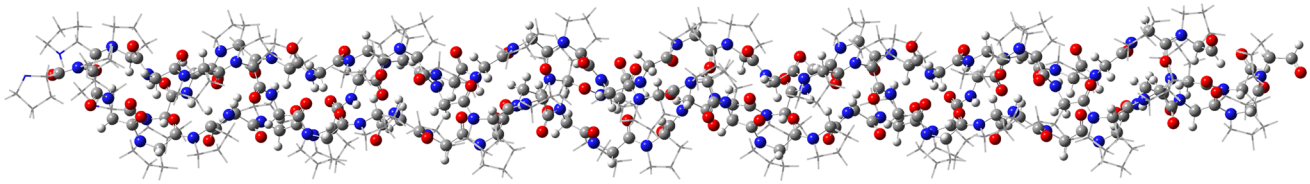

FIG. 4. The collagen triple helix $[(\text{Pro-Pro-Gly})_{10}]_3$ model used in the third case study.

molecules from Ref. 13 $(H_3C)_2N{-}(CH{=}CH)_4{-}NO_2$ [m−7] and $(H_3C)_2N{-}(C{\equiv}C)_4{-}NO_2$ [m−8].

The second case study concerns three fluorescent proteins: the so-called eGFP, SHardonnay, and DsRed, which were characterized experimentally and theoretically for their SHG properties.[22,23,37,50,51] SHardonnay was the first fluorescent protein especially designed to produce enhanced SHG values.[22] All these three proteins are derivatives of the green fluorescent protein where the protein β-barrel encapsulates the chromophore. To characterize them theoretically, two different models were considered: I. the chromophore only (Fig. 2), keeping the same conformation as in the protein, that was previously characterized at the TDHF, TDDFT, and MP2 levels of theory and II. the chromophore surrounded by its first shell of residues (including water molecules and amino acids from the protein-barrel, see Fig. 3) that was treated using the multi-layer ONIOM MP2:HF method in Refs. 22 and 23. Here, we used the first type of model to assess performances of sTD-DFT for β values in comparison with BHandHLYP/6-31+G(d) results. The second and larger models were used to characterize the performance of the sTD-DFT-xTB method and compared to ONIOM MP2:HF reference values.

In the last part, we used a model of a collagen triple helix $[(\text{Pro-Pro-Gly})_{10}]_3$ (PPG10, see Fig. 4) where in a previous publication, comparisons were made between ONIOM HF:HF and LC-BLYP:HF results[38] and experiment.[52] This model serves to assess the performance of the sTD-DFT-xTB method to characterize the SHG first hyperpolarizability of a large biochemical system.

One quantity which is usually extracted from hyper-Rayleigh scattering experiments is β_{HRS}.[4] Since this quantity encompasses all β-tensor components, it was systematically evaluated and discussed here. The β_{HRS} is defined as the mean of β-tensor orientations

$$\beta_{\text{HRS}}(-2\omega;\omega,\omega) = \sqrt{\left\{\left\langle\beta^2_{ZZZ}\right\rangle + \left\langle\beta^2_{ZXX}\right\rangle\right\}}, \tag{33}$$

where molecular averages without assuming Kleinman's conditions[53] are defined in the laboratory frame as

$$\begin{aligned}\left\langle\beta^2_{ZZZ}\right\rangle = {} & \frac{1}{7}\sum_{\zeta}^{x,y,z}\beta^2_{\zeta\zeta\zeta} + \frac{4}{35}\sum_{\zeta\neq\eta}^{x,y,z}\beta^2_{\zeta\zeta\eta} + \frac{2}{35}\sum_{\zeta\neq\eta}^{x,y,z}\beta_{\zeta\zeta\zeta}\beta_{\zeta\eta\eta} + \frac{4}{35}\sum_{\zeta\neq\eta}^{x,y,z}\beta_{\eta\zeta\zeta}\beta_{\zeta\zeta\eta} + \frac{4}{35}\sum_{\zeta\neq\eta}^{x,y,z}\beta_{\zeta\zeta\zeta}\beta_{\eta\eta\zeta} + \frac{1}{35}\sum_{\zeta\neq\eta}^{x,y,z}\beta^2_{\eta\zeta\zeta} \\ & + \frac{4}{105}\sum_{\zeta\neq\eta\neq\xi}^{x,y,z}\beta_{\zeta\zeta\eta}\beta_{\eta\xi\xi} + \frac{1}{105}\sum_{\zeta\neq\eta\neq\xi}^{x,y,z}\beta_{\eta\zeta\zeta}\beta_{\eta\xi\xi} + \frac{4}{105}\sum_{\zeta\neq\eta\neq\xi}^{x,y,z}\beta_{\zeta\zeta\eta}\beta_{\xi\xi\eta} + \frac{2}{105}\sum_{\zeta\neq\eta\neq\xi}^{x,y,z}\beta^2_{\zeta\eta\xi} + \frac{4}{105}\sum_{\zeta\neq\eta\neq\xi}^{x,y,z}\beta_{\zeta\eta\xi}\beta_{\eta\zeta\xi},\end{aligned} \tag{34}$$

and

$$\left\langle \beta^2_{ZXX} \right\rangle = \frac{1}{35}\sum_{\zeta}^{x,y,z}\beta^2_{\zeta\zeta\zeta} + \frac{4}{105}\sum_{\zeta\neq\eta}^{x,y,z}\beta_{\zeta\zeta\zeta}\beta_{\zeta\eta\eta} - \frac{2}{35}\sum_{\zeta\neq\eta}^{x,y,z}\beta_{\zeta\zeta\zeta}\beta_{\eta\eta\zeta} + \frac{8}{105}\sum_{\zeta\neq\eta}^{x,y,z}\beta^2_{\zeta\zeta\eta} + \frac{3}{35}\sum_{\zeta\neq\eta}^{x,y,z}\beta^2_{\zeta\eta\eta} - \frac{2}{35}\sum_{\zeta\neq\eta}^{x,y,z}\beta_{\zeta\zeta\eta}\beta_{\eta\zeta\zeta} + \frac{1}{35}\sum_{\zeta\neq\eta\neq\xi}^{x,y,z}\beta_{\zeta\eta\eta}\beta_{\zeta\xi\xi} - \frac{2}{105}\sum_{\zeta\neq\eta\neq\xi}^{x,y,z}\beta_{\zeta\zeta\xi}\beta_{\eta\eta\xi} - \frac{2}{105}\sum_{\zeta\neq\eta\neq\xi}^{x,y,z}\beta_{\zeta\zeta\eta}\beta_{\eta\xi\xi} + \frac{2}{35}\sum_{\zeta\neq\eta\neq\xi}^{x,y,z}\beta^2_{\zeta\eta\xi} - \frac{2}{105}\sum_{\zeta\neq\eta\neq\xi}^{x,y,z}\beta_{\zeta\eta\xi}\beta_{\eta\zeta\xi}. \tag{35}$$

In addition, from these quantities, the depolarization ratio can be obtained,

$$\mathrm{DR} = \frac{I^{2\omega}_{VV}}{I^{2\omega}_{HV}} = \frac{\left\langle \beta^2_{ZZZ} \right\rangle}{\left\langle \beta^2_{ZXX} \right\rangle}. \tag{36}$$

All reported β values are given in a.u. [1 a.u. of $\beta = 3.6213 \times 10^{-42}$ m^4 V^{-1} = 3.2064×10^{-53} C^3 m^3 J^{-2} = 8.639×10^{-33} esu] within the Taylor series convention.[54] The TD-DFT β calculations were computed using GAMESS quantum chemistry program.[39,40]

IV. RESULTS

A. Push-pull π-conjugated compounds

Push-pull π-conjugated molecules exhibit enhanced first hyperpolarizabilities modulated by donor-acceptor groups and the nature of their π-conjugated pathways. The six prototypical molecules [m−1 to m−6] were investigated at BHandHLYP/6-31G(d) and 6-31+G(d) levels of theory using TD-DFT as reference for comparison with sTD-DFT results and evaluated for thirteen different wavelengths (photon energies): 632 (1.96), 670 (1.85), 713 (1.74), 751 (1.65), 794 (1.56), 855 (1.45), 929 (1.33), 1240 (1.00), 1064 (1.17), 1500 (0.83), 1900 (0.65), 4133 (0.30), and ∞ (0) nm (eV). Note that for an amount of exact exchange of 0.5, y_K = 1.66 and y_J = 1.115. sTD-DFT calculations require an energy cut-off parameter as input related to the truncation of the CI space. This parameter was originally designed to truncate the excitation space in a way that excited states below that energy value are reasonably accurate. For the evaluation of β, the response equations converge for an energy cutoff above 10.0 eV. For safety reason and since it does not increase much the amount of CPU time, we chose an energy cutoff of 15.0 eV. Note that to achieve the same accuracy using the sum-over-state expression, one needs to include many more high-lying states up to at least 50.0–100.0 eV, increasing significantly the computation time. For example, to compute the polarizability mean of m−1 with a truncation parameter of 15.0 eV, using response theory 92% of the non-truncated calculated value is recovered, while using the sum-over-state expression we have only 65% of it.

Before discussing numerical results, it is noted that the most important requirement for the proposed method should be its ability to deal with off-resonance β responses. In a hyper-Rayleigh scattering experiment, after measuring the

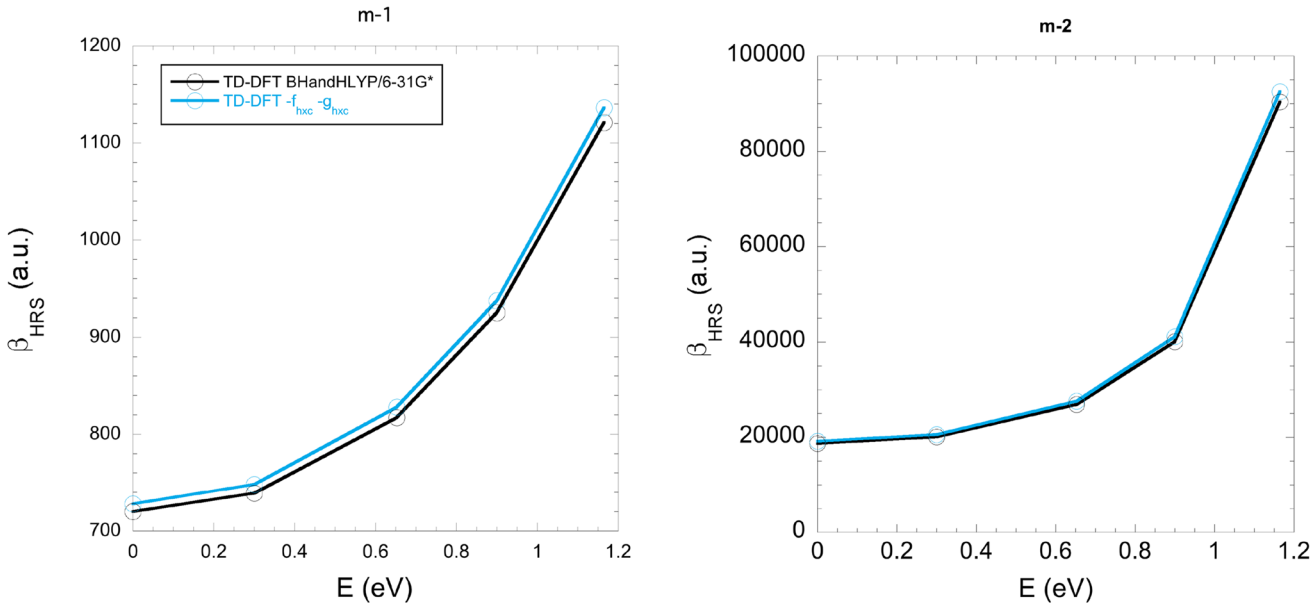

FIG. 5. Frequency dispersion of β_{HRS} for $H_2N{-}CH{=}CH{-}CH{=}CH{-}NO_2$ [m−1] and $(H_3C)_2N{-}(CH{=}CH)_6{-}NO_2$ [m−3] calculated using BHandHLYP TD-DFT method with 6-31G(d) basis set. In blue, the *C* term and the Hartree exchange-correlation kernel are neglected.

dynamic β_{HRS} of a solution, the next step is to extrapolate the static response by removing resonance enhancements, using an approximated scheme as the two-state approximation or more refined models.[55] This makes the static β, a crucial parameter to compare theory to experiment. From a theoretical point view, this workflow seems safer than directly

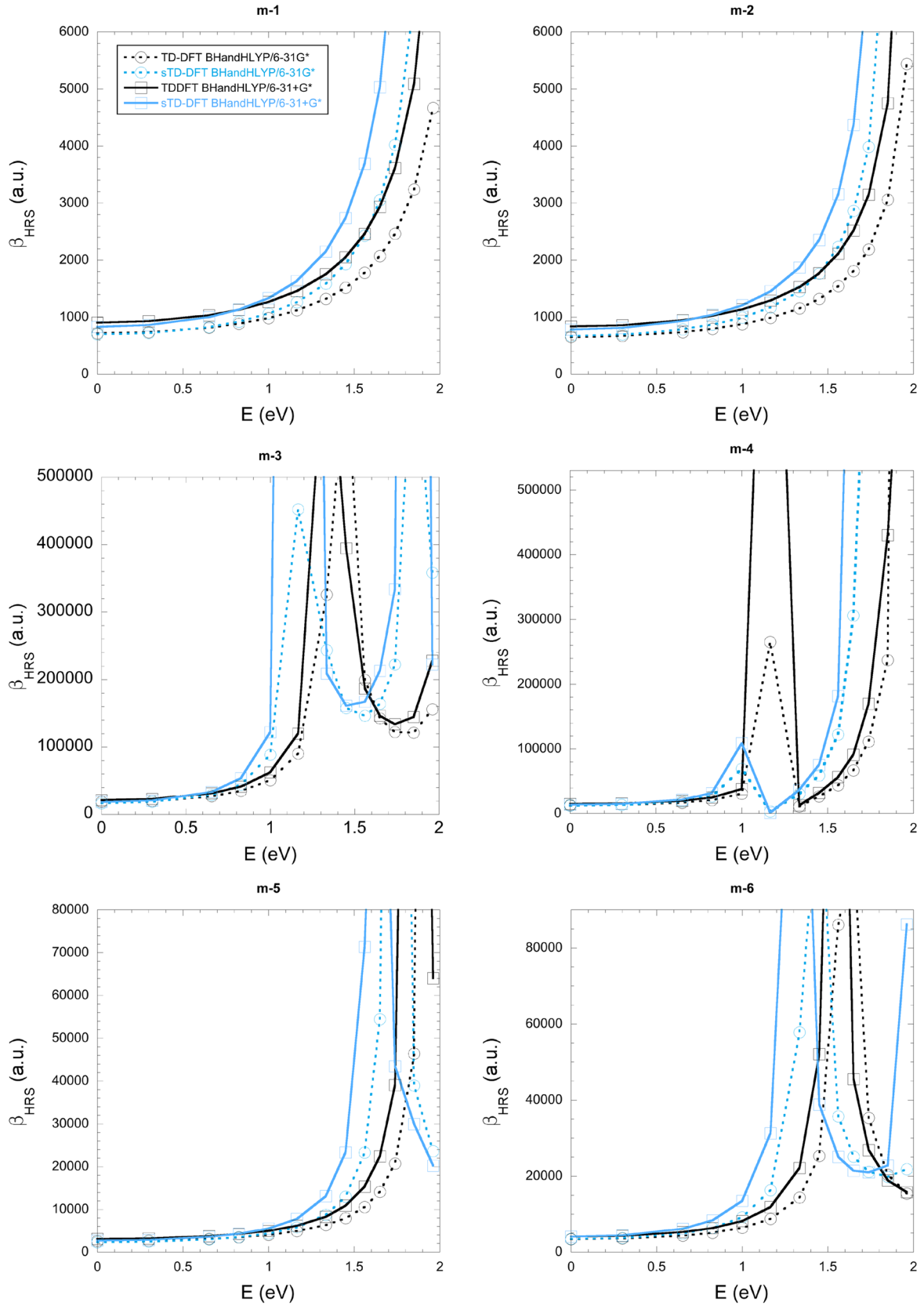

FIG. 6. Frequency dispersion of β_{HRS} for $H_2N-CH=CH-CH=CH-NO_2$ [m−1], $H_2N-C\equiv C-C\equiv C-NO_2$ [m−2], $(H_3C)_2N-(CH=CH)_6-NO_2$ [m−3], $(H_3C)_2N-(C\equiv C)_6-NO_2$ [m−4], *N*,*N*-dimethyl-4-(4-nitrophenyl)aniline [m−5], and *N*,*N*-dimethyl-5-(5-nitrothiophen-2-yl)thiophen-2-amine [m−6] calculated using BHandHLYP TD-DFT and sTD-DFT methods with 6-31G(d) and 6-31+G(d) basis sets.

comparing β values at the experimental wavelength because resonance enhancements are difficult to handle due to the divergent nature of response equations in the near-resonance regime.

Another point that needs to be discussed, is the validity of the two approximations to obtain the sTD-DFT first hyperpolarizability expression [Eq. (30)]. We have modified the TD-DFT implementation in GAMESS by neglecting the C term and the Hartree exchange-correlation kernel, like in the sTD-DFT implementation. Figure 5 presents the comparison of TD-DFT β values obtained with and without these approximations, for m−1 and m−3, at wavelengths of ∞, 4133, 1900, 1378, and 1064 nm. While these approximations really speed up the calculation by almost a factor of two (in our unoptimized modified version of GAMESS), the accuracy loss is negligible. These preliminary results indicate that quantum chemistry packages may implement this approach to allow users to benefit from these approximations, to avoid evaluating the very costly Hartree exchange-correlation kernel. Further tests of these approximations which can also be beneficial for the determination of two-photon absorption cross sections are ongoing in our laboratory.

Figure 6 presents TD-DFT and sTD-DFT β_{HRS} frequency dispersions. Globally, the sTD-DFT static β_{HRS} seem to be very similar to TD-DFT ones. Considering the 6-31G(d) basis set, static TD-DFT β_{HRS} values are overestimated by 2.8%, 2.5%, and 0.9% for m−1, m−2, and m−6, respectively, and underestimated by 11.9%, 3.0%, and 10.0%, for m−3, m−4, and m−5, respectively. At the 6-31+G(d) level, the sTD-DFT method underestimates TD-DFT reference values by 6.41%, 14.2%, 6.2%, 11.6%, and 0.1% for m−2, m−3, m−4, m−5, and m−6, respectively. Only the m−1 value is overestimated by 9.0%. With increasing frequency, the correlation between TD-DFT and sTD-DFT remains quite good up to 1.0 eV. Above that value, resonance enhancements are entering into the game and are difficult to handle for the sTD-DFT default parameterization. A reparameterization may improve the results, but it cannot be expected that the monopole approximation used to approximate the two-electron integrals can describe correctly all types of excitations/deexcitations implied in the β scattering process at high energies. While this method provides a good description of charge-transfer transitions,[31] by increasing the frequency, other types of excitation/deexcitation processes play a role, like transition to higher Rydberg states, for example. In Fig. 6, for m−4, one can observe that around 1 eV the resonance enhancement of TD-DFT is largely underestimated by sTD-DFT. To alleviate this, a multipole scheme for the two-electron integrals is currently under investigation.

sTD-DFT computation times for hyperpolarizabilties with an energy cutoff of 15.0 eV are much smaller than TD-DFT ones as shown in Fig. 7. The TD-DFT and sTD-DFT BHandHLYP/6-31G(d) calculations in Fig. 7 were done on the same 8 cores desktop computer (Intel core i7-6700, 3.40 GHz). The reduction of the number of basis functions after the CI-space truncation by the sTD-DFT method is also shown. For m−1, the sTDA program used 0.01 min to compute the static β_{HRS} value, while GAMESS needed 4.35 min to compute it. Note that the GAMESS implementation does not allow to compute a list of frequencies, meaning that for each requested frequencies, **A** and **B** matrices need to be recomputed each time. The sTD-DFT calculation for m−3 took 0.67 min, and the TD-DFT one took 30.9 min. This impressive reduction of computational time and the ability to characterize off-resonance first hyperpolarizabilties with a relatively good accuracy makes the sTD-DFT method a good choice to screen huge sets of compounds and to characterize large systems, routinely not accessible by standard TD-DFT.

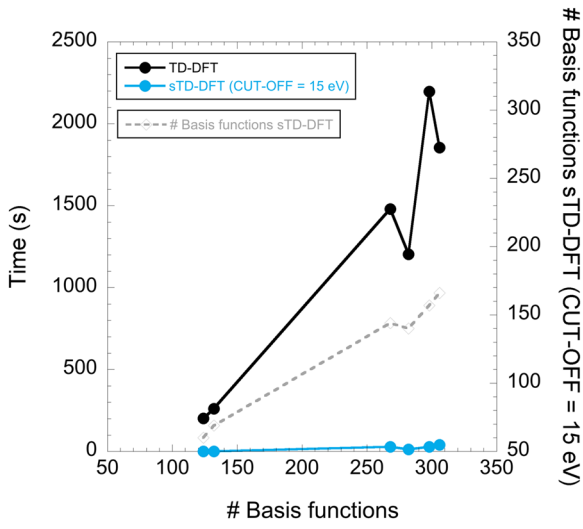

FIG. 7. Computation times at both TD-DFT and sTD-DFT levels using BHandHLYP functional and 6-31G(d) basis set as a function of the number of basis functions. The number of basis functions after truncation of the CI space by the sTD-DFT method is also provided. All the calculations were done on the same 8 cores desktop computer (Intel core i7-6700, 3.40 GHz).

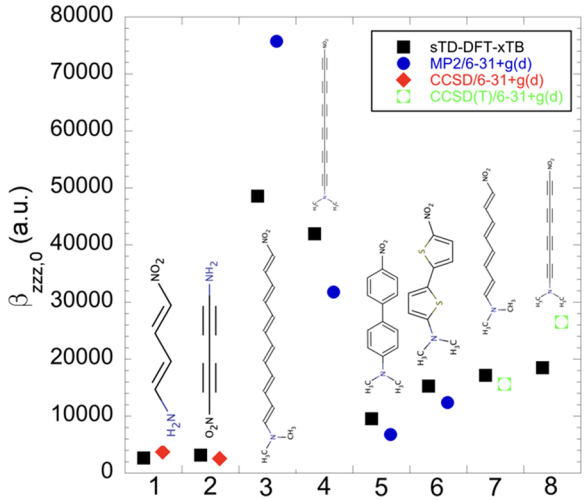

FIG. 8. Static β_{zzz} component for $H_2N{-}CH{=}CH{-}CH{=}CH{-}NO_2$ [m−1], $H_2N{-}C{\equiv}C{-}C{\equiv}C{-}NO_2$ [m−2], $(H_3C)_2N{-}(CH{=}CH)_6{-}NO_2$ [m−3], $(H_3C)_2N{-}(C{\equiv}C)_6{-}NO_2$ [m−4], *N*,*N*-dimethyl-4-(4- nitrophenyl)aniline [m−5], *N*,*N*-dimethyl-5-(5-nitrothiophen-2-yl)thiophen-2-amine [m−6], $(H_3C)_2N{-}(CH{=}CH)_4{-}NO_2$ [m−7], and $(H_3C)_2N{-}(C{\equiv}C)_4{-}NO_2$ [m−8] obtained at the sTD-DFT-xTB level of theory and compared to MP2, CCSD, and CCSD(T)/6-31+G(d) reference values.[13,36]

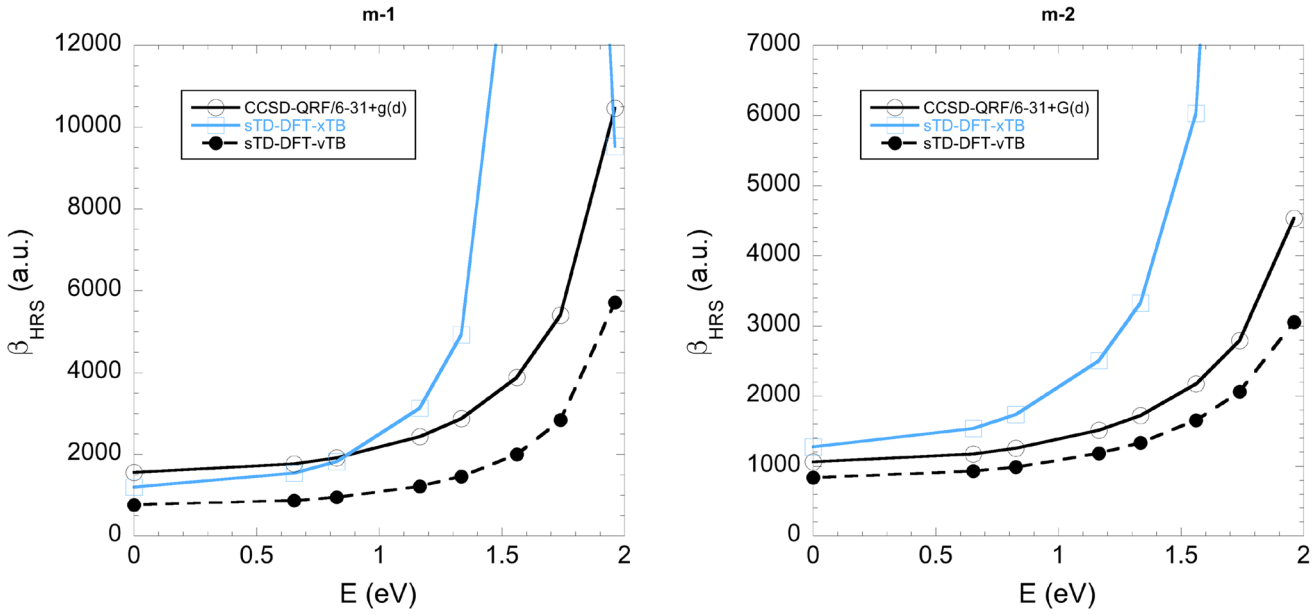

FIG. 9. Frequency dispersion of β_{HRS} for $H_2N{-}CH{=}CH{-}CH{=}CH{-}NO_2$ [m−1] and $H_2N{-}C{\equiv}C{-}C{\equiv}C\text{-}NO_2$ [m−2] calculated using sTD-DFT-vTB and -xTB methods and compared to CCSD-QRF/6-31+G(d) reference values.[36]

Figure 8 presents static β_{zzz} components computed at the sTD-DFT-xTB level of theory for eight push-pull molecules in comparison to high-level reference [MP2, CCSD, and CCSD(T)] data.[13,36] Note that the z direction is along the π-conjugation pathway, and that β_{zzz} component has the largest response. Considering the level of approximation of sTD-DFT-xTB, the purpose of this comparison is to test its ability mainly to reproduce trends in a series of similar compounds. The calculations presented in Fig. 8, all took less than a couple of minutes for computing the full tensor. In 2011, the computation of the static value of β at the CCSD(T)/6-31+G(d) level for only one component took several months using the finite-field method for m−7 and m−8.[13] The comparison is straightforward showing that the sTD-DFT-xTB method reproduces trends in a set of push-pull molecules, except for m−1 and m−2, but the difference is small. Considering the level of approximation, the amplitude of the response is well reproduced for m−1, m−2, m−5, m−6, and m−7, with −28.2%, 22.8%, 40.8%, 23.2%, and 10.1% difference, respectively. These differences are still lower than when using the HF method or most of DFT exchange-correlation functionals.[13,36] Figure 9 compares the β_{HRS} frequency dispersion for m−1 and m−2 obtained at the sTD-DFT-vTB, -xTB, and CCSD/6-31+G(d) levels of theory. vTB means that the diffuse AO basis functions have been removed from the xTB basis set, leaving only valence functions. Frequency dispersion curves are best described by the smaller basis set but reference β_{HRS} values are systematically under-evaluated. For m−1, the inclusion of diffuse functions improves the results for responses below 1.0 eV. Above that energy, however, xTB overestimates it. The basis set used in the xTB method could probably be improved to evaluate such properties, like by including polarization functions, but those are costly. As intermediate conclusion, the sTD-DFT-xTB method represents a very cheap way to evaluate frequency dependent first hyperpolarizabilities. This method is able to predict trends of β response values of push-pull π-conjugated molecules.

B. Fluorescent proteins

The next test case concerns three fluorescent proteins showing large SHG responses. For the chromophore geometries (Fig. 2), we computed BHandHLYP/6-31+G(d) TD-DFT and sTD-DFT β_{HRS} responses at the five wavelengths 1064 (1.17), 1378 (0.90), 1900 (0.65), 4133 (0.30), and ∞ (0) nm (eV). To improve the match with the TD-DFT results, we tuned the y_J parameter (called β in the original publication) on a small model of the FP chromphore (Fig. 10) and obtained an optimum y_J value of 0.83. Figure 11 presents results for eGFP, SHardonnay, and DsRed, as well as for the FP model. With the default parameters, sTD-DFT overestimates the static β_{HRS} by 22.0%, 23.8%, 32.6%, and 20.2% for the FP model, eGFP, SHardonnay, and DsRed. Tuning the y_J parameter reduces the difference to −0.14%, 3.7%, and −10.5%, for eGFP, SHardonnay, and DsRed. The aim of this was to show that to screen a set of similar compounds, a small parameter adjustment can dramatically improve the results. Doing the adjustment on a small model compound and applying it to larger molecules seem to

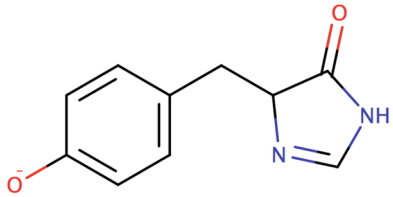

FIG. 10. Fluorescent protein chromophore model used to tune the Coulomb parameter y_J.

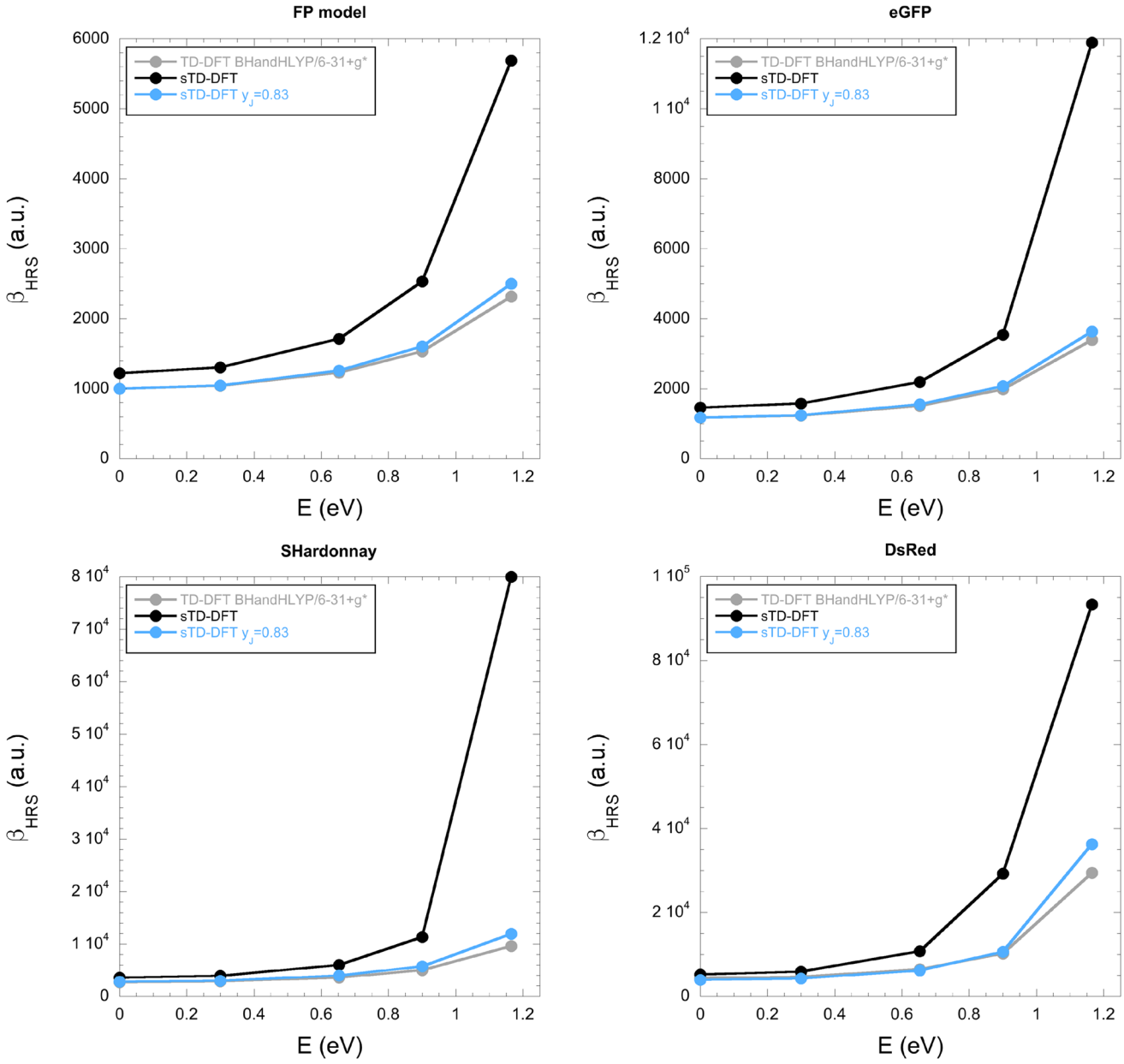

FIG. 11. Frequency dispersion of β_{HRS} for chromophore models, eGFP, SHardonnay, and DsRed, calculated using BHandHLYP TD-DFT (in gray) and sTD-DFT (in black) methods with 6-31+G(d) basis set. The blue line shows sTD-DFT results where the y_J parameter is optimized to best reproduce chromophore model TD-DFT values.

be a reasonable general workflow to improve the accuracy of the sTD-DFT method.

Considering the sTD-DFT-xTB method, Fig. 12 compares static β_{HRS} values to HF, BHandHLYP, and MP2/6-31+G(d) values,[22,23,37] for eGFP, SHardonnay, and DsRed chromophores. While for eGFP, the MP2 reference is best reproduced by BHandHLYP with a 5% over-estimation, SHardonnay and DsRed BHandHLYP values under-estimate MP2 β_{HRS} by 50% and 45%, respectively. sTD-DFT-xTB outperforms HF and BHandLYP, for SHardonnay and DsRed, with β_{HRS} values, 38% and 24%, lower with respect to the MP2 level of theory.

Figure 13 presents sTD-DFT-xTB static β_{HRS} results on the larger systems, i.e., eGFP, SHardonnay, and DsRed chromophores surrounded by their first shell of residues, which were previously investigated at the ONIOM MP2:HF/6-31+G(d) level of theory.[22,23] Note that such ONIOM calculations took half a year to be completed on a 12 CPU computer node. For the sTD-DFT-xTB calculation, the energy cutoff to truncate the CI space was set to 10.0 eV. For the eGFP model, it took 1.7 h to compute three sTD-DFT-xTB β_{HRS} values at 1064, 1900, and ∞ nm. Only the static results are presented here since it was not possible to determine the frequency dispersion at the MP2 level. For SHardonnay, the ONIOM MP2:HF reference is under-estimated by 6% using the sTD-DFT-xTB method. For eGFP and DsRed, reference values are over-estimated by 32% and 30%, respectively. Trends in this set of systems are similar at both levels of theory. These results

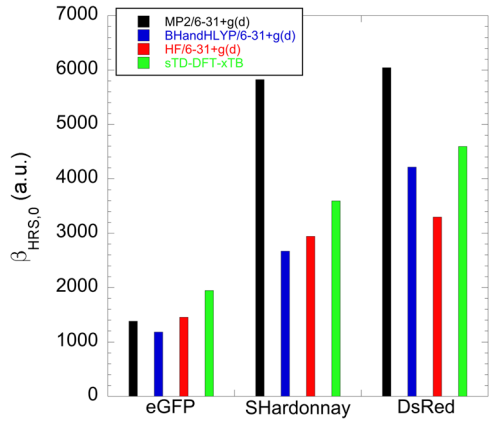

FIG. 12. Static β_{HRS} values for eGFP, SHardonnay, and DsRed chromophores obtained at the sTD-DFT-xTB level of theory and compared to HF, BHandHLYP, and MP2/6-31+G(d) reference values.[22,23,37]

are very promising for an ultra-fast computation of the first hyperpolarizability for large systems with a relatively good accuracy.

C. Collagen model

Figure 14 presents the β_{HRS} frequency dispersion of the PPG10 collagen model at the sTD-DFT-xTB level compared to ONIOM HF/6-31+G(d):HF/6-31G(d) and LC-BLYP/6-31+G(d):HF/6-31G(d) results taken from a previous investigation.[38] As for the large fluorescent protein models, a truncation parameter of 10.0 eV was used. While both ONIOM calculations took several months to obtain the β_{HRS} data, it only took less than two days for sTD-DFT-xTB method. The static sTD-DFT-xTB β_{HRS} value is only 8% lower than the ONIOM HF/6-31+G(d):HF/6-31G(d) value and 10% lower than the LC-BLYP/6-31+G(d):HF/6-31G(d) result. The sTD-DFT-xTB β_{HRS} frequency-dispersion curve is very similar to the one obtained at the LC-BLYP/6-31+G(d):HF/6-31G(d) level of theory. Note that this model system is composed of 1035 atoms. This result clearly demonstrates the potential of the sTD-DFT-xTB method for an ultra-fast treatment of large biological systems.

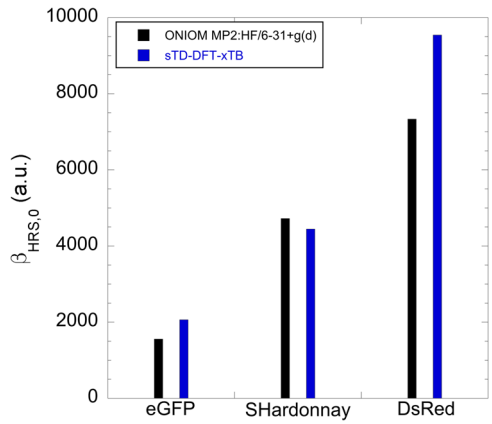

FIG. 13. Static β_{HRS} for eGFP, SHardonnay, and DsRed chromophores and their first shell of surrounding residues obtained at the sTD-DFT-xTB level of theory and compared to ONIOM MP2:HF/6-31+G(d) reference values.[22,23]

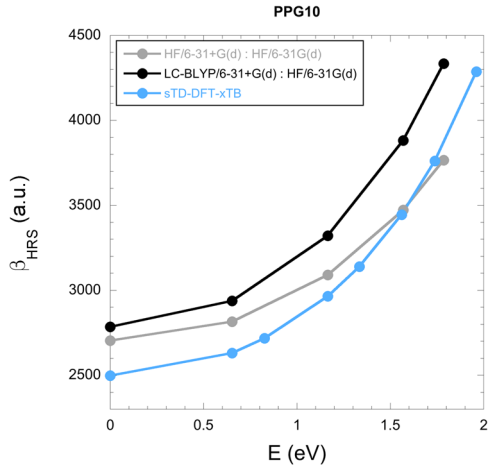

FIG. 14. Frequency dispersion of β_{HRS} for PPG10, calculated at the sTD-DFT-xTB level of theory and compared to ONIOM HF/6-31+G(d):HF/6-31G(d) and LC-BLYP/6-31+G(d):HF/6-31G(d) results.[38]

V. CONCLUSIONS AND OUTLOOKS

In this article, we have presented a first sTD-DFT implementation to evaluate first hyperpolarizability values for molecules. This method approximates the standard linear TD-DFT response equations by three simplifications: neglect of the XC functional response, monopole approximation of Coulomb and exchange integrals, and truncation of the CI space. In addition to this, to evaluate the quadratic response, we neglect the Hartree XC kernel and the third derivative of the XC functional. As shown for two push-pull π-conjugated compounds, these two approximations do not lead to any significant loss of accuracy but speed up the calculations by almost a factor of two. They should be further tested in regular TD-DFT implementations. In addition to the sTD-DFT method, a tight-binding version (sTD-DFT-xTB) was also tested. We challenged our implementation on three test cases: push-pull π-conjugated compounds, fluorescent proteins, and a collagen model, consisting of 1035 atoms. For push-pull systems, below a frequency-dispersion at about 1.0 eV, the sTD-DFT results are very similar to TD-DFT ones. Above that value, resonance enhancements are not so well treated. A reparameterization of the integral approximation parameters could help to correct this, but while the monopole approximation accurately describes valence and charge-transfer excitation/de-excitation processes, it is not necessarily the case for excitations which are more relevant at higher energies. Nevertheless, the sTD-DFT-xTB method computes trends between static β values for a set of push-pull π-conjugated molecules, well showing its ability to screen a large set of compounds, qualitatively and inexpensively. In the case of fluorescent proteins, two types of systems were investigated: the chromophore in its natural conformation to test sTD-DFT and sTD-DFT-xTB methods, and the chromophore with its first shell of residues to challenge the sTD-DFT-xTB capability to treat large systems. By slightly tuning the y_J parameter for the Coulomb integrals on a small chromophore model, we were able to dramatically improve the description in comparison to TD-DFT in its regular or simplified formulations, even at 1064 nm excitation frequency.

The comparison between reference MP2/6-31+G(d) calculations and sTD-DFT-xTB results shows that sTD-DFT-xTB outperforms HF and BHandHLYP, for SHardonnay and DsRed chromophores. Considering the larger systems, the sTD-DFT-xTB method was able to reproduce the trends with respect to the ONIOM MP2:HF calculations, while the evaluation of β was completed ultra-fast. Finally, for the collagen model, in a couple of days, sTD-DFT-xTB was able to provide a β frequency dispersion curve similar to the ONIOM LC-BLYP:HF one with a static β_{HRS} only 8% lower. This result shows the capability of the sTD-DFT-xTB method for an ultra-fast treatment of complicated electronic properties in large biological systems.

ACKNOWLEDGMENTS

This work was supported by the DFG in the framework of the "Gottfried-Wilhelm-Leibniz" prize.

[1] C. Stringari, L. Abdeladim, G. Malkinson, P. Mahou, X. Solinas, I. Lamarre, S. Brizion, J.-B. Galey, W. Supatto, R. Legouis, A.-M. Pena, and E. Beaurepaire, Sci. Rep. **7**, 3792 (2017).
[2] P. J. Campagnola and L. M. Loew, Nat. Biotechnol. **21**, 1356 (2003).
[3] M. G. Kuzyk and C. W. Dirk, *Characterization Techniques and Tabulations for Organic Nonlinear Optical Materials* (Marcel Dekker, 1998).
[4] T. Verbiest, K. Clays, and V. Rodriguez, *Second-Order Nonlinear Optical Characterization Techniques: An Introduction* (CRC Press, 2009).
[5] F. S. Pavone and P. J. Campagnola, *Second Harmonic Generation Imaging* (CRC Press, 2013).
[6] J. E. Reeve, H. L. Anderson, and K. Clays, Phys. Chem. Chem. Phys. **12**, 13484 (2010).
[7] L. Sacconi, D. A. Dombeck, and W. W. Webb, Proc. Natl. Acad. Sci. U. S. A. **103**, 3124 (2006), http://www.pnas.org/content/103/9/3124.full.pdf.
[8] A. L. A. Mascaro, L. Silvestri, L. Sacconi, and F. S. Pavone, IEEE Photonics J. **5**, 0701006 (2013).
[9] J. B. Shear, C. Xu, and W. W. Webb, Photochem. Photobiol. **65**, 931 (1997).
[10] K. C. Neuman, E. H. Chadd, G. F. Liou, K. Bergman, and S. M. Block, Biophys. J. **77**, 2856 (1999).
[11] D. M. Bishop, P. Norman, and H. S. Nalwa, *Nonlinear Optical Materials in Handbook of Advanced Electronic and Photonic Materials and Devices* (Academic Press, Burlington, 2001).
[12] M. G. Papadopoulos, A. J. Sadlej, and J. Leszczynski, *Non-Linear Optical Properties of Matter* (Springer, 2006).
[13] M. de Wergifosse and B. Champagne, J. Chem. Phys. **134**, 074113 (2011).
[14] J. R. Hammond and K. Kowalski, J. Chem. Phys. **130**, 194108 (2009).
[15] K. Y. Suponitsky, S. Tafur, and A. E. Masunov, J. Chem. Phys. **129**, 044109 (2008).
[16] B. Champagne and B. Kirtman, J. Chem. Phys. **125**, 024101 (2006).
[17] M. de Wergifosse, V. Liégeois, and B. Champagne, Int. J. Quantum Chem. **114**, 900 (2014).
[18] J. Quertinmont, B. Champagne, F. Castet, and M. H. Cardenuto, J. Phys. Chem. A **119**, 5496 (2015).
[19] M. H. Cardenuto and B. Champagne, J. Chem. Phys. **141**, 234104 (2014).
[20] M. H. Cardenuto and B. Champagne, Phys. Chem. Chem. Phys. **17**, 23634 (2015).
[21] S. Dapprich, I. Komáromi, K. Byun, K. Morokuma, and M. J. Frisch, J. Mol. Struct.: THEOCHEM **461-462**, 1 (1999).
[22] E. De Meulenaere, N. Nguyen Bich, M. de Wergifosse, K. Van Hecke, L. Van Meervelt, J. Vanderleyden, B. Champagne, and K. Clays, J. Am. Chem. Soc. **135**, 4061 (2013).
[23] M. de Wergifosse, E. Botek, E. De Meulenaere, K. Clays, and B. Champagne, J. Phys. Chem. B **122**, 4993 (2018).
[24] A. Zangwill and P. Soven, Phys. Rev. A **21**, 1561 (1980).
[25] S. Hirata and M. Head-Gordon, Chem. Phys. Lett. **314**, 291 (1999).
[26] F. Furche, J. Chem. Phys. **114**, 5982 (2001).
[27] F. Wang, C. Y. Yam, and G. Chen, J. Chem. Phys. **126**, 244102 (2007).
[28] A. J. Thorvaldsen, K. Ruud, K. Kristensen, P. Jørgensen, and S. Coriani, J. Chem. Phys. **129**, 214108 (2008).
[29] F. Zahariev and M. S. Gordon, J. Chem. Phys. **140**, 18A523 (2014).
[30] S. M. Parker, D. Rappoport, and F. Furche, J. Chem. Theory Comput. **14**, 807 (2018).
[31] S. Grimme, J. Chem. Phys. **138**, 244104 (2013).
[32] C. Bannwarth and S. Grimme, "Excited states: From isolated molecules to complex environments," Comput. Theor. Chem. **1040-1041**, 45 (2014).
[33] S. Grimme and C. Bannwarth, J. Chem. Phys. **145**, 054103 (2016).
[34] S. Nénon and B. Champagne, J. Chem. Phys. **138**, 204107 (2013).
[35] S. Nénon and B. Champagne, J. Phys. Chem. Lett. **5**, 149 (2014).
[36] M. de Wergifosse, "Quantum chemical investigations of nonlinear optical compounds: From model to complex systems for second harmonic imaging microscopy," Ph.D. dissertation (Université de Namur, 2014).
[37] E. De Meulenaere, I. Asselberghs, M. de Wergifosse, E. Botek, S. Spaepen, B. Champagne, J. Vanderleyden, and K. Clays, J. Mater. Chem. **19**, 7514 (2009).
[38] M. de Wergifosse, J. de Ruyck, and B. Champagne, J. Phys. Chem. C **118**, 8595 (2014).
[39] M. W. Schmidt, K. K. Baldridge, J. A. Boatz, S. T. Elbert, M. S. Gordon, J. H. Jensen, S. Koseki, N. Matsunaga, K. A. Nguyen, S. Su, T. L. Windus, M. Dupuis, and J. A. Montgomery, J. Comput. Chem. **14**, 1347 (1993).
[40] M. S. Gordon and M. W. Schmidt, in *Theory and Applications of Computational Chemistry*, edited by C. E. Dykstra, G. Frenking, K. S. Kim, and G. E. Scuseria (Elsevier, Amsterdam, 2005), pp. 1167–1189.
[41] See http://www.turbomole.com for "TURBOMOLE V6.2 2010, a development of University of Karlsruhe and Forschungszentrum Karlsruhe GmbH, 1989-2007, TURBOMOLE GmbH, since 2007."
[42] K. Nishimoto and N. Mataga, Z. Phys. Chem. **12**, 335 (1957).
[43] K. Ohno, Theor. Chim. Acta **2**, 219 (1964).
[44] G. Klopman, J. Am. Chem. Soc. **86**, 4550 (1964).
[45] D. C. Ghosh and N. Islam, Int. J. Quantum Chem. **110**, 1206 (2010).
[46] D. A. Kleinman, Phys. Rev. **126**, 1977 (1962).
[47] A. D. Becke, J. Chem. Phys. **98**, 1372 (1993).
[48] P. C. Hariharan and J. A. Pople, Theor. Chim. Acta **28**, 213 (1973).
[49] M. M. Francl, W. J. Pietro, W. J. Hehre, J. S. Binkley, M. S. Gordon, D. J. DeFrees, and J. A. Pople, J. Chem. Phys. **77**, 3654 (1982).
[50] E. D. Meulenaere, M. de Wergifosse, E. Botek, S. Spaepen, B. Champagne, J. Vanderleyden, and K. Clays, J. Nonlinear Opt. Phys. Mater. **19**, 1 (2010).
[51] E. D. Meulenaere, M. de Wergifosse, E. Botek, J. Vanderleyden, B. Champagne, and K. Clays, AIP Conf. Proc. **1642**, 522 (2015).
[52] A. Deniset-Besseau, J. Duboisset, E. Benichou, F. Hache, P.-F. Brevet, and M.-C. Schanne-Klein, J. Phys. Chem. B **113**, 13437 (2009).
[53] R. Bersohn, Y. Pao, and H. L. Frisch, J. Chem. Phys. **45**, 3184 (1966).
[54] A. Willetts, J. E. Rice, D. M. Burland, and D. P. Shelton, J. Chem. Phys. **97**, 7590 (1992).
[55] J. Campo, W. Wenseleers, E. Goovaerts, M. Szablewski, and G. H. Cross, J. Phys. Chem. C **112**, 287 (2008).